Vol. 723: 185–200, 2023
https://doi.org/10.3354/meps14315

MARINE ECOLOGY PROGRESS SERIES
Mar Ecol Prog Ser

Published November 23[§]

Contribution to the Theme Section 'Wind and weather effects on seabird foraging, movement and energetics'

Thermal soaring over the North Sea and implications for wind farm interactions

Jens van Erp[1,*,#], Elspeth Sage[1,#], Willem Bouten[1], Emiel van Loon[1], Kees C. J. Camphuysen[2], Judy Shamoun-Baranes[1]

[1]Department of Theoretical and Computational Ecology, Institute for Biodiversity and Ecosystem Dynamics, University of Amsterdam, 1090 GE Amsterdam, The Netherlands

[2]Royal Netherlands Institute for Sea Research (NIOZ) Texel, 1790 AB Den Burg (Texel), The Netherlands

ABSTRACT: Seabirds use several flight modes at sea, including thermal soaring, in which thermal uplift is used to gain altitude and save energy. An increase in flight altitude may have consequences for wind farm interactions if it results in birds spending more time within the rotor-swept zone (RSZ). To understand conditions under which thermal soaring occurs and potential implications for wind farm interactions, we investigated thermal soaring in relation to atmospheric conditions in June and July at 2 study areas in the North Sea, west and north of the Dutch coast. We developed algorithms that identified thermal soaring in GPS tracks of lesser black-backed gulls *Larus fuscus* and radar tracks of seabirds. By combining species-specific 3-dimensional information on flight behaviour from bio-logging with the continuous spatiotemporal coverage of radar positioned at wind parks, we obtained a more comprehensive overview of thermal soaring at sea than either method would obtain alone. Our results showed that birds flew at higher altitudes during thermal soaring than non-soaring flight, increasing the proportion of flight time within the RSZ. Thermal soaring occurred inside offshore wind farms to a similar degree as outside. Thermal soaring was positively correlated with positive temperature differences (ΔT) between sea surface and air (at 2 m above sea level), and north and north-westerly winds. We show that the probability of thermal soaring over the North Sea, inside and outside wind farms, increases with larger temperature differences, resulting in increased time spent within the RSZ and an increased collision risk for seabirds.

KEY WORDS: Offshore wind farm · Thermal convection · Bird radar · GPS telemetry · Seabirds · Gulls · Human–wildlife interactions

1. INTRODUCTION

Marine environments are undergoing extensive change as a result of human activities, including large infrastructure developments such as rapid growth of offshore wind industry (Esteban & Leary 2012). Seabirds already face multiple conservation threats (Croxall et al. 2012), and wind farms may place additional pressures on their survival through a range of direct and indirect effects (Perrow 2019). One of these effects is the collision of birds with wind turbines, which can increase mortality (Marques et al. 2014). Estimates of collision partially depend on the spatial overlap between the birds and the turbine rotors, which is mostly determined by 2 key metrics: the flight altitude distribution and some measure of bird density in the area (Band 2012, Kleyheeg-Hartman et al. 2018). Generally, seabird flight altitude offshore is low (Johnston et al. 2014, Ross-Smith et al. 2016), but seabirds gain altitude when performing thermal soaring (Woodcock 1940a, 1975, Pennycuick 1983, Weimerskirch et al. 2003), an energy-saving flight

*Corresponding author: j.a.vanerp@uva.nl
#These authors contributed equally to this work

§Advance View was available June 15, 2023.
This corrected version: December 21, 2023. For details see www.int-res.com/abstracts/meps/v723/c_p185-200/

Publisher: Inter-Research · www.int-res.com

mode (Nourani & Yamaguchi 2017), which could increase the probability of flying through the rotor-swept zone (RSZ) of wind turbines. Thermal soaring flight is therefore especially relevant when considering interactions with wind turbines, and such interactions have been studied among soaring birds on land (Péron et al. 2017, Hanssen et al. 2020), but not at sea.

The influence of atmospheric conditions on thermal soaring has mainly been studied on land (Nourani & Yamaguchi 2017), but comparable interactions also take place at sea. When cooler air overlies a warmer sea surface, the air warms up and expands, destabilising the lower atmosphere and creating vertical movement of the warm air as thermals. The difference between sea surface temperature (SST) and air temperature (T_a) as (SST − T_a, or ΔT) is a suitable proxy for thermal uplift (Haney & Lee 1994, Woodcock 1940a) and is important in facilitating sea crossings by raptors around the world (Nourani et al. 2021). Changes in the altitude profile of birds during thermal soaring depend, among other factors, on both the strength of available thermals, as well as species morphology and behaviour (Pennycuick 2008). Thermal soaring at sea is well described in tropical latitudes, where occurrence of thermals is predictable enough that frigatebirds have developed a flight specialisation enabling them to use thermal soaring flight to stay aloft for weeks on open water (Weimerskirch et al. 2016). Raptors also use thermal soaring in sea crossings at higher latitudes during migration (Yamaguchi et al. 2012, Nourani et al. 2020, 2021), and it is possible that thermal soaring is used more widely over temperate waters than past research indicates.

One of the most important areas for offshore wind energy production in Europe is the North Sea, a shallow shelf sea located in North-Western Europe. Here offshore wind development has been growing at an accelerating pace and is projected to grow considerably in the future (Rijksoverheid 2019, European Commission 2020). As a result, considerable effort has gone into measuring seabird behaviour, including studies of flight paths, flight altitude and turbine avoidance behaviour (Krijgsveld et al. 2011, Johnston et al. 2014, Ross-Smith et al. 2016), all of which aim to improve the understanding of how wind farm developments may impact seabirds (Marques et al. 2014, Thaxter et al. 2019). Thermal soaring, however, has never been examined empirically over the North Sea, although several seabird species present in the North Sea can use thermals. In particular, larids such as lesser black-backed gulls *Larus fuscus* and herring gulls *L. argentatus* are flight generalists that commonly use flapping flight (Ainley et al. 2015, Shamoun-Baranes et al. 2016), but their morphology allows them to take advantage of thermal updrafts to support soaring flight (Lindhe Norberg 2002, Sage et al. 2022). Herring gulls have been observed thermal soaring in tropical and lower mid-latitudes over the western Atlantic Ocean (Woodcock 1940b), and lesser black-backed gulls are able to use thermal soaring and orographic soaring over land (Shamoun-Baranes et al. 2016, Sage et al. 2019) and soaring flight over sea (Shamoun-Baranes et al. 2016). Thus, under suitable environmental conditions, they may use thermal soaring in temperate marine environments such as the North Sea.

The aims of this paper were to determine how thermal soaring at sea influences the flight altitude distributions of birds, to identify whether thermal soaring occurs within wind farm areas, and to better understand how weather conditions promote thermal soaring at sea, all in the context of collision risk assessments for wind farms. To achieve our aims, we combined 2 tracking techniques which provide complementary information. We used biologging data (GPS and accelerometry) to study the 3D flight behaviour at sea of lesser black-backed gulls from 2 coastal populations situated 24 and 60 km from 2 offshore wind farms (Luchterduinen and Gemini windpark, respectively). However, obtaining a large enough sample size for data analysis within offshore wind farms is challenging. We therefore combined analysis from radars, positioned at both offshore wind farms, which provide continuous coverage of flight behaviour of all birds in the vicinity, but lack altitude and species-specific information. Additionally, both datasets were used to investigate the influence of ΔT and wind direction on thermal soaring in order to understand the atmospheric conditions facilitating thermal soaring at sea. We expected higher flight altitudes and an increased proportion of flight time spent within the RSZ during thermal soaring. We had no clear expectation as to whether thermal soaring occurrence within wind farms would differ from occurrence outside, as it is unclear how thermal uplift and intrinsic motivation for thermal soaring is affected by the wind farm. Furthermore, we expected positive ΔT to promote thermal soaring and that these conditions mainly develop when winds from higher latitudes cause a decrease in T_a. For additional insight into the conditions promoting thermal uplift, we describe the synoptic weather system during one particular time period of intense thermal soaring activity, thereby linking broad-scale weather

patterns to fine-scale flight behaviour. Finally, we discuss the effect of thermal soaring behaviour on collision risk in offshore wind farms and possibilities for integration into future offshore wind farm planning.

2. MATERIALS AND METHODS

2.1. Study area and study period

The study was conducted over the southern North Sea (Fig. 1) between 52 and 55° N latitude, a temperate area characterised by shallow sea depths <40 m (NOAH 2022). GPS and radar measurements were taken in 2 study areas, to the west and north of the Dutch coast (Fig. 1). We refer to the 2 study areas as the west and north area. To get an overview of the species flying in these areas and relate them to the radar data (which is non-species specific) we gathered species counts from European Seabirds at Sea (ESAS) 5.0 ship survey data (Reid & Camphuysen 1998), which are reported in Tables S1 & S2 in the Supplement at www.int-res.com/articles/suppl/m723p185_supp/. The study was conducted from June through July in 2019 and 2020. SST ranged from 280 to 297 K (average 290.0 K in the west area and 288.9 K in the north area) and T_a ranged from 281 to 302 K (average 289.6 K in the west area and 288.6 K in the north area) (based on ERA5, see Section 2.4).

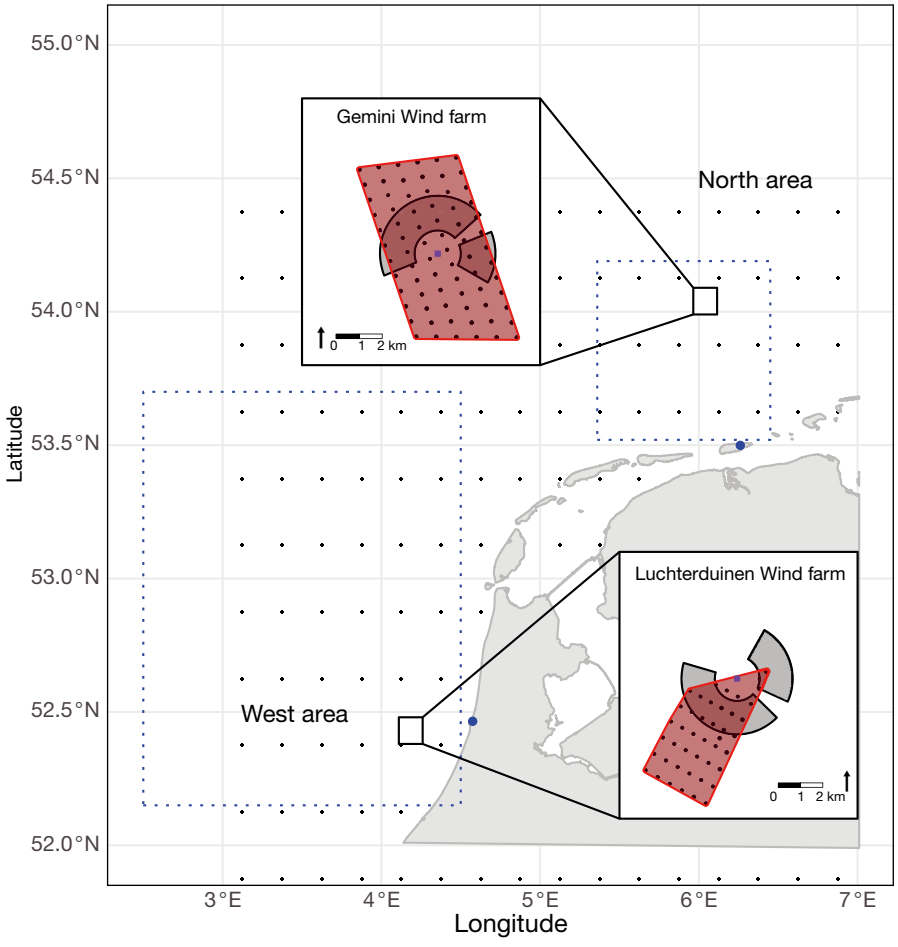

Fig. 1. Overview of the 2 study areas (west and north, relative to the Dutch coast). Blue dots show the lesser black-backed gull colonies at IJmuiden (west) and Schiermonnikoog (north), and dotted squares show the geographical fence for high-resolution GPS capture. Small black squares show the location of Luchterduinen (west) and Gemini (north) wind farms. Close-up views of the 2 wind farms show individual turbines (black dots) within the defined wind farm area (red outlined area), radar location (purple square) and spatial measurement range of the radars (grey shaded area). Black gridded dots across the sea area show corners of ERA5 grid cells

2.2. Lesser black-backed gull tracking data and analysis

GPS and accelerometer data were used to identify thermal soaring at sea by individual lesser black-backed gulls and to examine the altitude profile of thermal soaring flight in comparison to flapping flight. These data were gathered using UvA-BiTS trackers (Bouten et al. 2013) fitted to individual lesser black-backed gulls at 2 breeding colonies in the west and north study area (Forteiland and Schiermonnikoog, respectively; Fig. 1) as part of long-term monitoring efforts. Individuals were tagged in 2017 and 2018 on Schiermonnikoog island (53.499° N, 6.261° E) and in 2019 and 2020 on Forteiland (4.575° N, 52.465° E), situated near IJmuiden on the mainland. The catching protocol followed previous protocols used for lesser black-backed gulls at Dutch study sites (Shamoun-Baranes et al. 2016), where birds were captured during incubation, fitted with trackers using a wing harness made of a Teflon ribbon threaded with a nylon string and released within 20 min of capture following tagging. All tagging was carried out in accordance with the Dutch ethics committee on animal experiments (DEC) of the Royal Netherlands Academy of Arts and Sciences (KNAW), and with permission by land managers PBN (IJmuiden) and Natu-

urmonumenten (Schiermonnikoog). The data acquisition program was set up to maximise high-resolution (3 s interval) measurements at sea by using a geographical fence for each colony. The fence covered the majority of the local marine foraging area per colony and triggered the high-resolution measurement protocol when a tagged individual moved inside (Fig. 1). GPS data collected within these 2 fences in the north and west area during June and July in 2019 and 2020 were used in this study. The trackers also collected tri-axial acceleration data at 20 Hz for 1 s following each GPS measurement. Acceleration measurements were used for behaviour classification using a random forest classifier described by Shamoun-Baranes et al. (2016), which identifies 11 different flight and non-flight behaviours. In this study, the main purpose of the behavioural classifier was to identify flight behaviour and distinguish flapping and soaring flight, where soaring is defined as a bird in flight and not flapping its wings (which includes climbing and gliding).

In order to identify thermal soaring by lesser black-backed gulls, high-resolution flight trajectories with reliable altitude measurements were required, which could resolve circular movement patterns and fine-scale altitude changes. Due to the use of a geographical fence, nearly all data were collected at high resolution. However, in some instances, lower-resolution data can be captured within the fence (e.g. if device battery voltage is low), so the point-to-point interval was calculated between every location (annotated to the second location), and any location with an interval ≥10 s was removed. Under the high-resolution measurement protocol, altitude errors of the UvA-BiTS trackers are relatively low with a mean measurement accuracy of 1.42–2.77 m at a measurement interval of 6 s (Bouten et al. 2013). Nevertheless, to minimise the effect of any anomalous altitudes, 3-dimensional point-to-point velocity was calculated between subsequent points, and where this velocity exceeded 50 m s^{-1}, the altitude was recalculated as the average of the altitudes to either side of the point. Measurements of altitude above sea level (a.s.l.) can also be systematically biased on a regional scale by the ellipsoid model for the Earth's surface upon which altitude (a.s.l.) is calculated. To estimate this bias, we investigated the altitude measurements of all GPS points with behaviour classified as 'floating', indicating positions at sea level. The mean altitude of all floating-point measurements (99 137 points) was −4.36 m, which was considered an approximation of the systematic error caused by the ellipsoid model. To correct for the error, this value was added to all GPS altitude measurements. To remove anomalous positional fixes, the point-to-point ground speed between locations was calculated using point-to-point distance and time interval. We considered 3117 points (0.028% of total) for which 2-dimensional ground speed exceeded 50 m s^{-1} as unrealistic anomalies and removed them. Following this filtering, data considered for further analysis consisted of 603.4 h of recorded flight time across 148 d and 18 individuals from the west area, with a mean time interval of 5 ± 0.2 s, and 357.6 h across 103 d and 12 individuals from the north area, with a mean time interval of 4.4 ± 1 s.

High-resolution GPS data were used to identify individual moments of thermal soaring by lesser black-backed gulls based on flight behaviour, flight speed and altitude gain. Interruptions occurred in the time series of high-resolution data whenever a bird left and then re-entered the high-resolution fence area. All points were therefore grouped into periods of uninterrupted high-resolution data, deemed 'bouts'. Bouts were classified by ascribing unique ascending ID numbers to every measurement (including the non-high-resolution data), then identifying breaks in subsequent measurements based on the ID numbers. Where interruptions of more than 4 subsequent measurements occurred in the high-resolution data (usually because a bird left the geographical fence area) this was deemed a break in uninterrupted high-resolution data, ending a bout. Within a bout, points were assigned 1 of 3 classifications: circling, i.e. periods of circling flight with a gain in altitude; gliding: i.e. periods of directional flight without flapping and with a loss or maintenance of altitude; and other, i.e. when neither of these behaviours was identified. To determine these classifications, a moving average approach was used. For each location, a 3-point (the location and 1 point to either side) moving average of climb rate (m s^{-1}), angular velocity (° s^{-1}), ground speed (m s^{-1}) and proportion of time spent soaring (as defined by accelerometer behavioural classification) was calculated. Where climb rate was >0 m s^{-1}, angular velocity was >10° s^{-1}, ground speed was >5 m s^{-1} and proportion of time spent soaring was ≥0.6, a point was defined as circling. This soaring proportion limit was chosen to allow for incidental flapping during soaring-dominant behaviours, which was commonly found in the data and is expected in gulls. Where climb rate was ≤0 m s^{-1}, ground speed was >5 m s^{-1} and proportion of time spent soaring was ≥0.6, a location was defined as gliding. Any series of gliding points that was not preceded by at least 1 circling point within a bout was re-classified as 'other', as there was no evidence of this gliding being connected to thermal soaring be-

haviour. Consecutive circling points were considered a circling bout, consecutive gliding points were considered a gliding bout, and a circling bout with its directly subsequent gliding bout was considered a thermal soaring bout. Thermal soaring bouts were identified in 26 individuals (all 18 individuals from the west area and 11 individuals from the north area).

To gain insight into the amount of time gulls spent in different flight modes and at different altitudes, time proportion metrics were calculated (such as the overall proportion of flight time spent in thermal soaring flight). The proportion of different flight behaviours taking place within the RSZ were also calculated. The RSZ altitude range was set at 25–150 m a.s.l. and chosen as a broadly representative RSZ for the 2 wind farms in this study (Luchterduinen, 25–137 m; and Gemini, 23.5–153.5 m a.s.l.). To account for the GPS altitude accuracy, confidence bounds for these values were also calculated based on adding or subtracting 3 m (rounded up from the mean accuracy reported by Bouten et al. 2013 to either limit of the RSZ (22–28 m lower range and 147–153 m upper range).

In order to compare the proportion of soaring with environmental conditions experienced, the hourly proportion of flight time spent in circling flight was calculated (circling time proportion). Here only circling flight was considered, rather than circling and gliding, as the occurrence of circling flight is expected to be most directly related to environmental conditions generating thermals. The final GPS data set consisted of data from the west area amounting to 938 covered hours across 115 d and data from the north area amounting to 586 covered hours across 82 d. In the west area, 2 individuals contributed data in both 2019 and 2020, whilst 5 individuals contributed data in both years in the north area. An overview of data counts per individual per year is presented in Table S3 (Section S2 of the Supplement).

2.3. Radar data and analysis

Radar data were used to identify and examine the extent of thermal soaring at 2 locations partly overlapping with offshore wind farms. Bird flight was monitored by 2 bird radar systems with a tracking algorithm (RobinRadar 3D Fixed). One system was mounted on the service platform of turbine 42 situated at the edge of the Luchterduinen wind farm (52.4278° N, 4.1853° E, 21.8 m a.s.l.), 23 km from the coast (west area; Fig. 1). A second system was mounted on the offshore power station of Gemini wind farm (54.0370° N, 6.0417° E, 31 m a.s.l.), situated 60 km north of Schiermonnikoog (north area; Fig. 1). The radar systems consisted of a vertically rotating X-band antenna (25 kW, Furuno Marine) and horizontally rotating S-band antenna (60 kW, Furuno Marine) both rotating at 0.75 rotations s^{-1}. For this study, only data captured by the horizontal antenna were used.

Radar measurements were automatically processed to create tracks of birds using proprietary software developed by RobinRadar and further post-processed to provide reliable observations as described by van Erp et al. (2021). Radar data were collected during June and July in 2019 and 2020 for the west area and in 2020 for the north area (as the north radar was not operational until 2020). The bird-detection probability of the radar is not equal over the whole radar observation window; therefore, data were sampled at 1000–2500 m from the radar, minus the area blocked by the structure on which the radar was installed and the area overlapping with the vertical antenna (between 287–30° and 115–135° in the west area and between 119–247° and 47–67° in the north area; see Fig. 1). The radar system only measures birds in flight, detecting birds reliably up to an altitude of 300 m for small birds (<62.5 g) and up to an altitude of 600 m for larger birds (500 g; see Fig. S1 in Section S3 of the Supplement).

Each track created by the radar software included at least 5 track points and several track properties: geolocation plus timestamp (UTC) per track point and track direction calculated between the first and last track point (radians). Track length (m) was calculated as the sum of the great circle distance between consecutive track points. Average ground speed (m s^{-1}) was calculated as track length divided by track duration (last timestamp – first timestamp, s). Average airspeed was calculated according to Shamoun-Baranes et al. (2007) using ground speed, track direction and hourly *u*- and *v*-wind components (at 10 m a.s.l.) retrieved from the ERA5 reanalysis dataset (see Section 2.4). Wind components were annotated to the tracks based on nearest hour to the calculated mid-point timestamp of the track (first timestamp + ½ track duration). Only tracks with an average airspeed between 5 and 30 m s^{-1} were included, as nearly all seabird species fly within this airspeed range (Spear & Ainley 1997a,b, Alerstam et al. 2007, Shamoun-Baranes et al. 2016). Additionally, manual data exploration indicated that static reflections from nearby vessels or structures created stationary, long-lasting, false positive bird tracks, which can differ per radar due to different surroundings and place-

ment height (a.s.l.). To automatically identify these clutter tracks, we calculated the displacement over time (m s^{-1}) by dividing the great circle distance between the first and last track point by the track duration. Through visual inspection, the tracks falling in the 1st percentile of displacement over time (0.66 m s^{-1}) and the 10th percentile of displacement over time (3.72 m s^{-1}) in the west and north datasets, respectively, were identified as clutter and removed. Additionally, to remove false positive bird tracks caused by reflections of the turbines in the nearby wind farm, any track with >80% of the positions occurring within 100 m radius of a turbine was also removed.

During the study period, the radar was occasionally not operational, and hours in which the radar was fully offline were not included in the analysis. Furthermore, exploratory analysis revealed that birds were no longer detected by the radar when the clutter filter of the radar was highly active. Therefore, to reduce the chance of analysing artificial lows in bird abundance caused by high filter activity, we removed all hours with an average filter activity above a set threshold of 0.327 for the west area and 0.311 for the north area (further explanation available in Fig. S2 in Section S4 of the Supplement). After applying the aforementioned selection criteria, 2265 h of data (2 379 356 tracks) remained for the west area over 113 d in 2019–2020, and 866 h of data (413 208 tracks) remained for the north area over 49 d in 2020.

In order to identify thermal soaring in the radar tracks, a method was developed to identify thermal soaring flight from information extracted from the 2D trajectory data collected by the radar. Point-to-point heading (flight direction relative to the air) was calculated based on hourly *u*- and *v*-wind components nearest to the point timestamp, point-to-point groundspeed and bearing (flight direction relative to the ground). From this, angular velocity was calculated per point as the change between subsequent point-to-point headings divided by point-to-point time steps. Circling flight was identified as a continuously turning track section (3-point average of angular velocity between 10 and 60° s^{-1}) for a minimum of 2 full circles (720°). Other tortuous behaviours, such as foraging, could also be identified as circling this way. As thermals are advected by wind, the net direction of circling flight within a thermal is expected to align with the wind direction (Treep et al. 2016, Weinzierl et al. 2016). Therefore, when wind speed was estimated high enough to cause advection which would distinguish thermal circling from other tortuous flight (wind speeds >2 m s^{-1}), the net direction of circling flight had to align within a 90° window of the wind direction (45° clock- and counter-clockwise) to be considered thermal soaring. Circling flight was identified in 10 676 out of 2 379 356 (0.0045%) tracks in the west area (2019 and 2020), and in 580 out of 413 208 tracks (0.0014%) in the north study area (2020).

To assess the extent of thermal soaring in offshore wind farms, circling tracks were counted both within and outside the wind farm area. A geometric box was drawn around the outer turbines of the wind farm plus a 100 m buffer (Fig. 1, red area). The area where the wind farm overlapped with the study area (Fig. 1, grey area) was considered inside the wind farm (west area 4.7 km^2, north area 9.0 km^2); the rest of the study area was considered outside the wind farm (west area 6.1 km^2, north area 0.7 km^2). Tracks were annotated by occurrence of circling in or outside the wind farm area. If circling occurred both inside and outside within a single track, the track was considered for both categories. Circling density (circling tracks per km^2) per day was calculated for both areas by dividing the number of circling tracks observed per day, per area, by the area size (km^2).

To analyse the relation between thermal soaring occurrence and the associated environmental conditions, we calculated hourly proportion of circling tracks (circling track proportion) by dividing the number of circling tracks per hour by the total number of tracks per hour occurring in the area of interest. All tracks occurring between xx-1:30:00 and xx:29:29 were included in hour xx. Note that for GPS, we consider circling time proportion, whereas for radar, we consider circling track proportion, which are similar but not completely equal measurements of thermal soaring. Where both data sets are considered, we simply refer to the data as 'circling proportions'.

2.4. Environmental conditions

In order to calculate wind-dependent track properties (Section 2.3) and to investigate the environmental conditions under which thermal soaring occurs, hourly measures of thermal soaring from GPS and radar were annotated with atmospheric and sea surface parameters. These parameters were acquired from the European Centre for Medium-Range Weather Forecast (ECMWF) ERA5 reanalysis, providing data on a regular latitude–longitude grid at 0.25° × 0.25° spatial resolution and hourly temporal resolution (Hersbach et al. 2020, 2022). Data were retrieved for the latitude–longitude box with coordinates 51–54.25° N and 3.25–7° E. The parameters extracted from ERA5 data were T_a at 2 m above sur-

face (T_a, K), SST (K), and *u*- and *v*-wind components at 10 m above surface (m s^{-1}). ΔT was calculated as SST – T_a.

Environmental variables (SST, T_a, ΔT and *u*- and *v*-components) were annotated to GPS points and radar tracks according to the nearest neighbour in time and space. SST and T_a were also examined independently of ΔT in order to investigate how their individual dynamics influence ΔT, particularly in the context of synoptic weather conditions. To provide insight into the synoptic scale conditions that may lead to positive ΔT, weather charts from the Royal Netherlands Meteorological Institute (Koninklijk Nederlands Meteorologisch Instituut) and time series of environmental variables from ERA5 (SST, T_a, wind speed) were examined throughout a specific thermal soaring peak (19–23 July 2020) and are presented in Figs. S3 & S4 in Section S5 of the Supplement.

2.5. Statistical analysis

All analyses were carried out in R (R Core Team 2022). To assess the extent to which the circling time proportion (GPS) and circling track proportion (radar) complemented each other per study area, we visualised the data temporally on a daily scale and calculated the Pearson correlation coefficient. To examine whether thermal soaring flight increases the chance of flying within the RSZ, GPS measurements were grouped based on flight mode (thermal soaring or non-thermal soaring) and altitude range (within RSZ altitude range or outside RSZ altitude range). A binomial logistic regression model was then fitted to the GPS data per study area (formula: altitude range ~ flight mode) where 'within RSZ' was considered presence and 'outside RSZ' absence, with individual as random effect, and evaluated for significant effects of flight mode on altitude range. Thermal soaring occurrence within and outside the wind farm areas was compared by calculating the daily difference between soaring density inside and outside the wind farm (removing days with no observed soaring to prevent zero-inflation of the data) and performing a 2-sided *t*-test (alternate hypothesis = mean is not equal to 0). To test if thermal soaring occurs more with positive ΔT, binomial logistic regression models were fitted to the data per measurement technique (formula: circling proportion ~ ΔT), with year as random factor and weighted (by number of observations per hour for radar data, and by total measured flight time per hour for GPS), and with a first-order autoregressive covariance structure to account for temporal autocorrelation. To relate thermal soaring occurrence to wind conditions, binomial logistic regression models were fitted to the data per measurement technique (formula: circling proportion ~ wind *u* × wind *v*) with year as random factor and weighted (by number of observations per hour for radar data, by total measured flight time per hour for GPS), and with a first-order autoregressive covariance structure to account for temporal autocorrelation. The binomial logistic regression models were implemented as 'glmm' using the R package 'MASS' (Venables & Ripley 2002) and evaluated through the 'R^2_{glmm}' (Nakagawa et al. 2017) using the R package 'MuMIn' (Burnham & Anderson 2002) which reports the marginal (mR^2_{glmm}) and conditional (cR^2_{glmm}) pseudo-R^2.

3. RESULTS

Proportions of circling were generally low, but varied among days, with some time periods having little or no soaring flight and other periods having large peaks that could last more than a day (Fig. 2). Some of these peaks occurred at the same time in both regions (e.g. around 8 June 2020 and 20 July 2020). In the west area, circling proportions were higher in July than in June for both years. Peaks in circling were less pronounced in the north radar circling track proportions during 2020, compared to other data. Note that in the north areas, no radar data were available during the entire period in 2019, and no GPS data were available in July 2019.

Correlation of circling time proportion and circling track proportion was 0.664 for the west coast data, and 0.153 for the north coast (2020 only), indicating an overlap in thermal soaring behaviour observed in lesser black-backed gulls measured with GPS and all birds measured with radar in the west area but not in the north.

3.1. Thermal soaring of lesser black-backed gulls measured with GPS tracking

The median proportion of time spent in flight across all individuals was 0.86 (IQR: 0.79–0.90) in the west area and 0.83 (IQR: 0.68–0.91) in the north area. The altitude distributions of non-thermal soaring flight and of thermal soaring flight followed a skewed distribution with a tail at greater altitudes (Fig. 3). The probability of flying within the RSZ increased during thermal soaring in both areas (binomial logistic re-

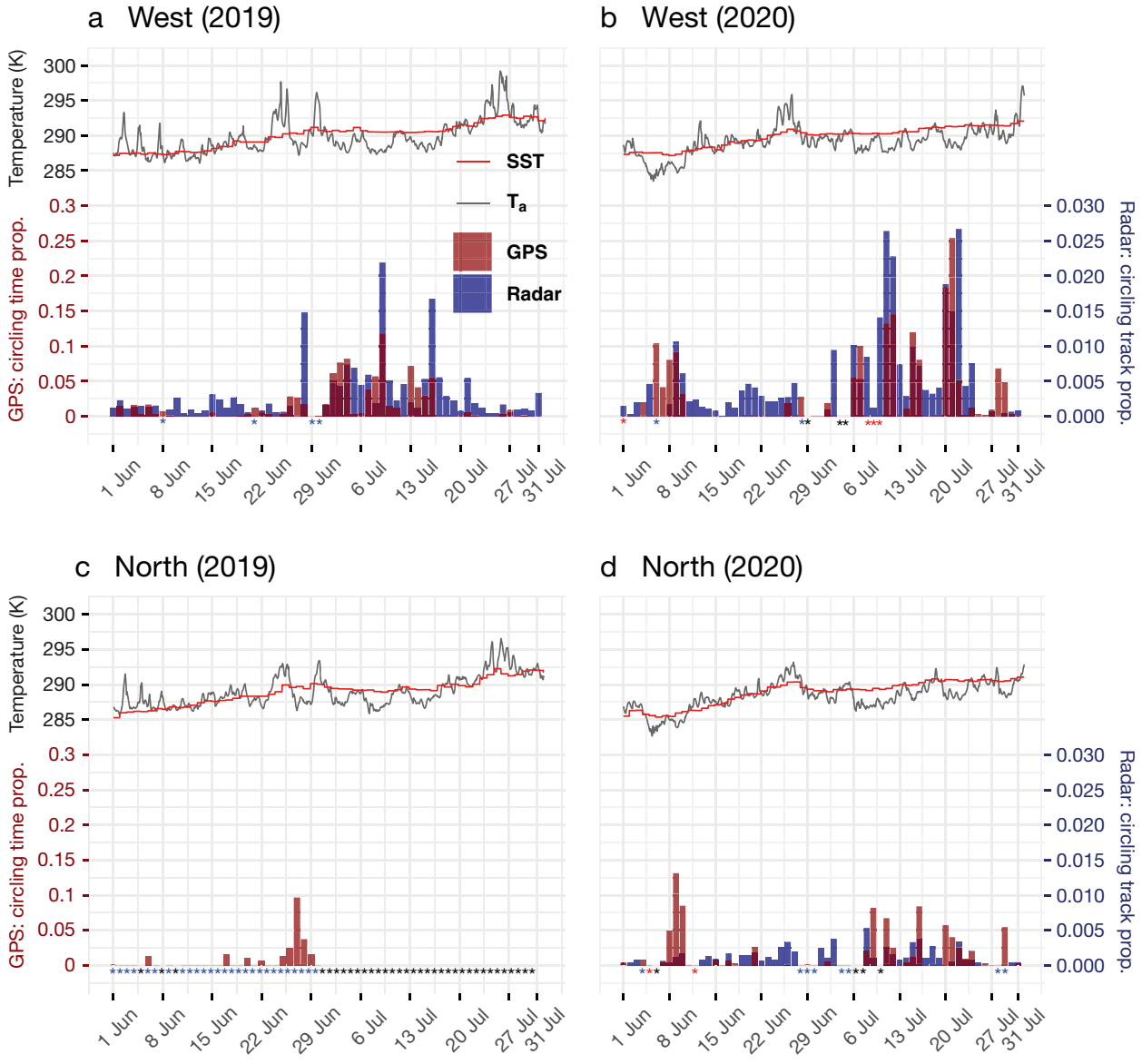

Fig. 2. Timeline of measured thermal soaring and associated environmental conditions. Daily circling time proportion for lesser black-backed gulls (GPS, red bars) and circling track proportion of all observed birds (radar, blue bars) are shown for the west area in (a) 2019 and (b) 2020 and for the north area in (c) 2019 (GPS data only) and (d) 2020. Dark red bars indicate the overlap between circling time and circling ratio. Hourly sea surface temperature (SST, red) and air temperature at 2 m a.s.l. (T_a, black) from the ERA5 reanalysis grid cell nearest to the respective radar locations are shown as line-graphs above each daily occurrence graph. Days without soaring data available are depicted by an asterisk below the *x*-axis (red, blue and black depict missing GPS, radar and both data, respectively)

gression; size estimate 1.815, $p < 0.001$, $mR^2_{glmm} = 0.024$, $cR^2_{glmm} = 0.122$, and 2.850, $p < 0.001$, $mR^2_{glmm} = 0.032$, $cR^2_{glmm} = 0.177$ for the west and north area, respectively). A summary of measured altitudes in non-thermal and thermal soaring flight, alongside summaries of the proportions of time spent in non-thermal and thermal soaring flight within the RSZ is reported in Table 1.

3.2. Thermal soaring measured through radar tracking

Observed circling density did not differ significantly between inside and outside the wind farm for the west area in both years (1-sample 2-sided *t*-test; 2019: n = 52, p = 0.876; 2020: n = 44, p = 0.714). In the north area, circling density was different between inside and out-

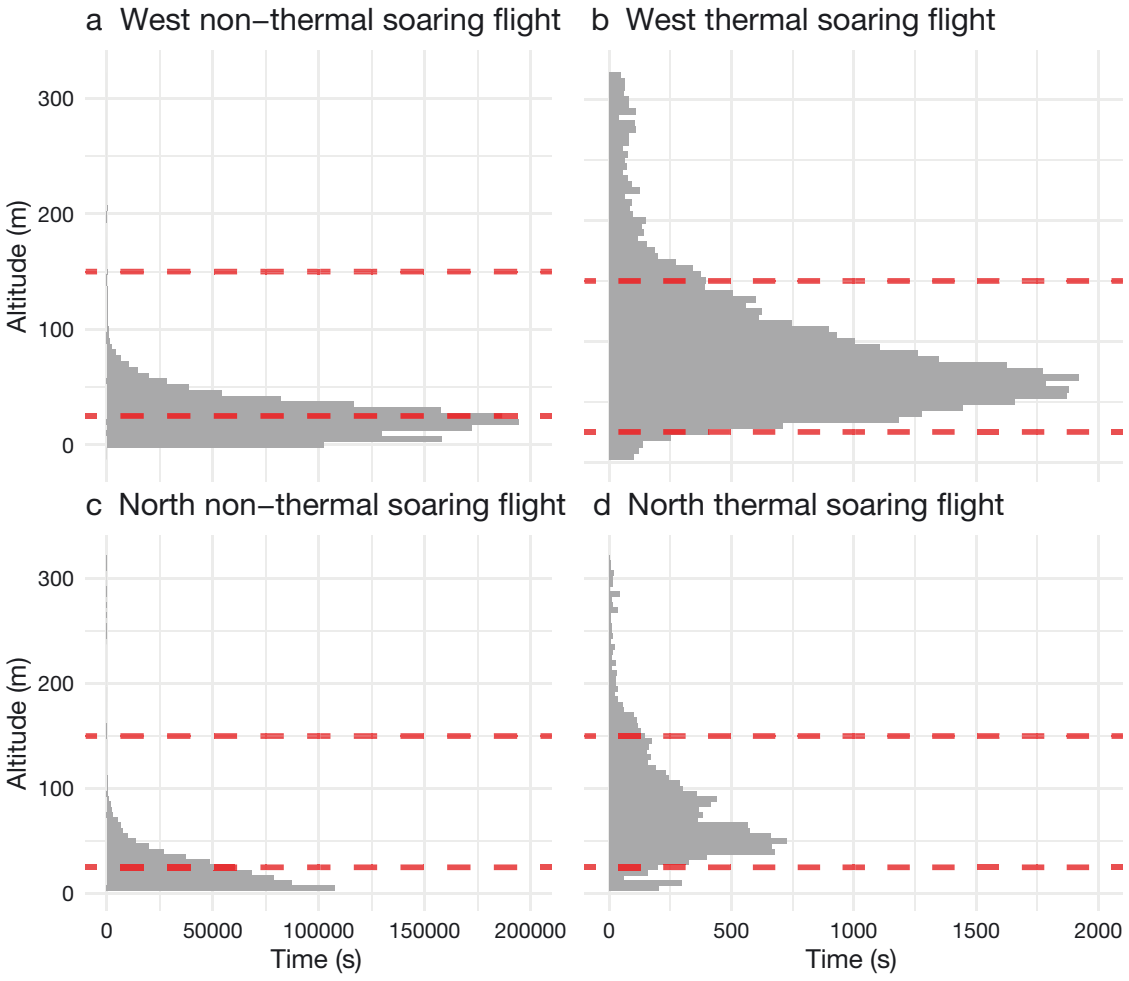

Fig. 3. Altitude distribution of (a,c) non-thermal soaring flight (all flight excluding thermal soaring bouts) and (b,d) thermal soaring flight for lesser black-backed gulls tracked in the (a,b) west and (c,d) north study areas across 2019 and 2020. Red dashed lines indicate typical minimum and maximum rotor-swept zone (RSZ) heights of turbines in the study area. Note that the range of the *x*-axes differs between non-thermal soaring flight (0–200000 s) and thermal soaring flight (0–2500 s)

Table 1. Summary of GPS data and key derived metrics relating to altitude and relative time spent in the rotor-swept zone (RSZ) for thermal and non-thermal soaring flight. Median values are presented with interquartile ranges (IQR) in brackets. Values relating to the proportion of time within the RSZ are presented with confidence bounds accounting for the GPS altitude accuracy in brackets

	West	North
GPS measurements (no.)	367668	256954
Individuals (no.)	18	12
Hours of data (no.)	511	311
Covered days (no.)	115	82
Median altitude (m) (non-thermal)	22.4 (IQR: 11.4–33.4)	12.4 (IQR: 2.4–26.4)
Median altitude (m) (thermal)	82.4 (IQR: 56.4–124.4)	70.37 (IQR: 45.4–112.4)
Proportion of all flight time within RSZ	0.44 (0.37–0.52)	0.28 (0.24–0.33)
Proportion of non-thermal soaring flight time in RSZ	0.36 (0.30–0 .43)	0.20 (0.17–0.23)
Proportion of thermal soaring flight time in RSZ	0.80 (0.79–0.81)	0.78 (0.76–0.80)
Proportion of total flight time defined as thermal soaring	0.034	0.022
Proportion of total flight time in RSZ defined as thermal soaring	0.062 (0.054–0.072)	0.061 (0.054–0.071)

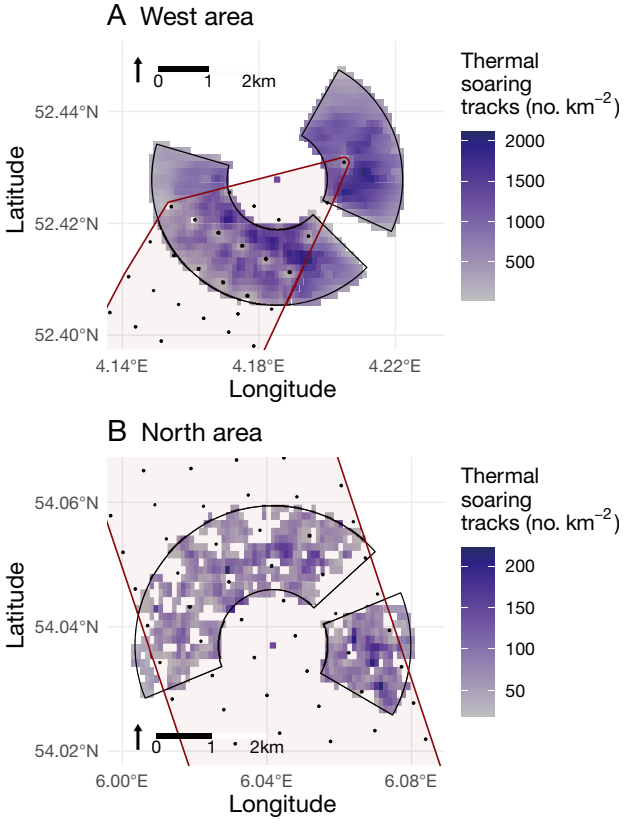

Fig. 4. Spatial distribution of circling density for the (a) west and (b) north radar area (100 × 100 m cells). Density (light to dark blue) scales differently per area to increase visual clarity; cells without observed circling are transparent. The west area shows the averaged density distribution for 2019 and 2020, the north area shows the distribution for 2020. The radar sampling area is outlined in black, with the turbine locations as black dots and the radar location in red. The wind farm area is outlined in red

side the wind farm (1-sample 2-sided *t*-test; n = 20, p = 0.022), with a mean difference below 0 (–0.768), indicating decreased thermal soaring inside the wind farm. Visualizations of circling densities show a patchy distribution in both areas (Fig. 4). In the west area, the highest circling density was observed closer to the radar and between the turbines, and lowest around the turbine locations and the edges of the sampling area. In the north area, the distribution was somewhat fragmented due to the smaller data set; nonetheless, circling was found throughout the area, including the small section outside the wind farm. A summary of radar tracking data and observed circling count and density is reported in Table 2.

3.3. Thermal soaring and environmental conditions

SST increased slightly throughout the season (Fig. 2), whilst T_a fluctuated more throughout the season in response to diurnal variation and synoptic weather patterns (Section S5 of the Supplement). Peaks in circling proportion typically occurred during periods when SST was higher than T_a (ΔT positive), especially for periods longer than 1 d (Fig. 2a,b). One such period can be seen following 8 June 2020, where a peak in soaring is observable in the west area (Fig. 2b) as well as the north area for GPS-tracked gulls (Fig. 2d). These peaks align with a period during which T_a dropped below SST for approximately 3 d. Similar alignments of thermal soaring peaks with positive ΔT are also noticeable in July 2020, with a particularly large peak observable in the west area based on GPS tracking and radar monitoring and in the north area based on GPS around 20 July. This peak is due to the passage of a cold front followed by a trough over the North Sea resulting in T_a dropping and remaining below SST for several days (Supplement Section S5, Figs. S3 & S4, Video S1).

The relation between circling proportion and environmental conditions was consistent across the GPS data and west radar data (Fig. 5, Table 3). ΔT had a significant positive effect on circling proportion (binomial logistic regression; west GPS: size estimate = 0.841, $p < 0.001$, $mR^2_{glmm} = 0.483$, $cR^2_{glmm} = 0.494$, north GPS: size estimate = 0.819, $p = 0.006$, $mR^2_{glmm} = 0.403$, $cR^2_{glmm} = 0.403$, west radar: size estimate = 0.557, $p < 0.001$, $mR^2_{glmm} = 0.207$, $cR^2_{glmm} = 0.236$), showing that thermal soaring increases with increasing ΔT. Wind *v*-components had a negative effect on circling proportion (binomial logistic regression; west GPS: size estimate = –0.272, $p < 0.001$, $mR^2_{glmm} = 0.255$, $cR^2_{glmm} = 0.275$, north GPS: size esti-

Table 2. Summary of radar tracking data and an overview of circling track count and density (tracks km^{-2}) identified for the west and north study areas. Tracks with circling identified both inside and outside the wind farm were counted for both categories (inside and outside)

	West 2019		West 2020		North 2020	
Tracks (n)	1 209 312		1 170 044		413 208	
Hours of data	1166		1099		866	
Covered days	57		56		49	
	Inside	Outside	Inside	Outside	Inside	Outside
Circling tracks (n)	1291	1714	3488	4713	550	39
Surface area (km^2)	4.7	6.1	4.7	6.1	9.0	0.7
Circling density (n km^{-2})	274	279	740	768	61	57

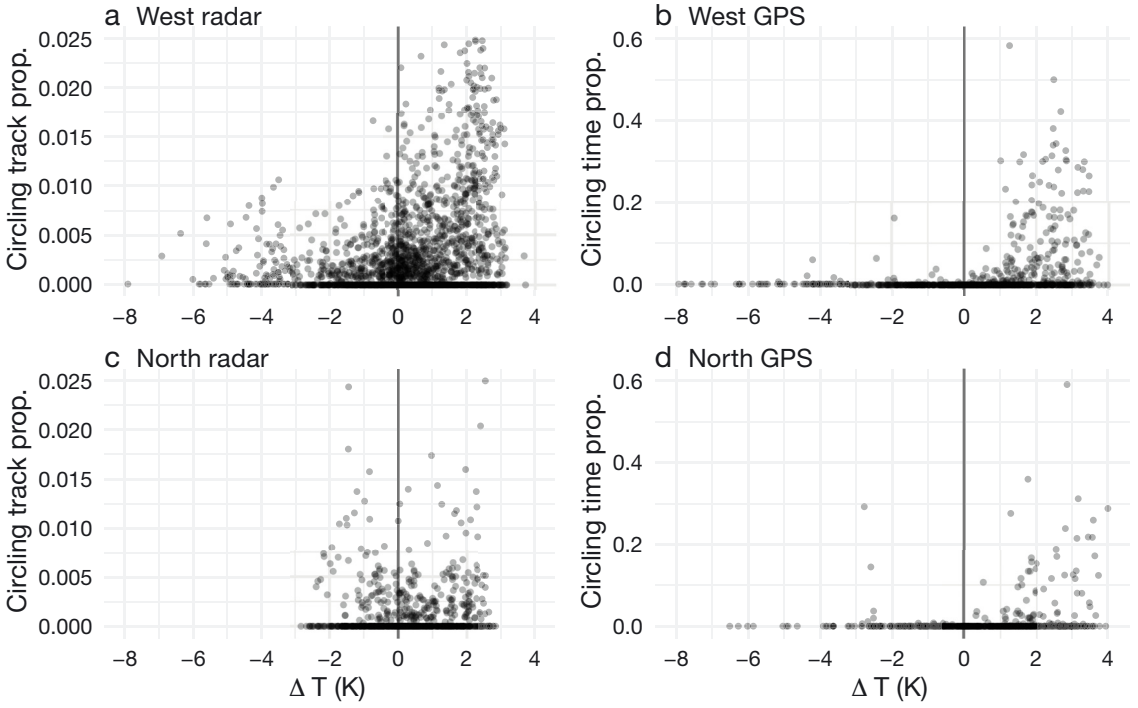

Fig. 5. Overview of hourly circling track proportion (radar; west = 2265 h, north = 866 h) and circling time proportion (GPS; west = 938 h, north = 586 h) and the local temperature difference between sea surface and air at 2 m a.s.l. (ΔT) in the same hour. The vertical line highlights the divide between negative and positive ΔT

mate = −0.174, p = 0.001, mR^2_{glmm} = 0.170, cR^2_{glmm} = 0.181, west radar: size estimate = −0.088, p = 0.001, mR^2_{glmm} = 0.038, cR^2_{glmm} = 0.092), indicating that thermal soaring increases with northerly winds. Additionally, wind *u*-components had a positive effect on circling proportion for the west area (binomial logistic regression; GPS: size estimate = 0.111, p = 0.004, radar: size estimate of 0.046, p = 0.025), indicating that thermal soaring increases with westerly winds as well. On average, circling proportion and ΔT were highest with positive *u*- and negative *v*-wind components, corresponding to north-westerly winds (Fig. 6a–c). Although the first-order autoregressive covariance structure reduced temporal autocorrelation in the residuals of the models, it could not be completely removed for the west radar (Section S6 in the Supplement), and more complex covariance structures provided no improvement. For the north area, no significant effects were found on hourly circling track proportion measured by radar.

4. DISCUSSION

This study shows that thermal soaring occurs over the North Sea, as measured by GPS tracking and radar in 2 areas during June and July. Flight altitudes were higher in lesser black-backed gulls during thermal soaring, resulting in a higher proportion of flight time spent within the RSZ, and thermal soaring occurred inside wind farms to a similar extent as outside. Together, these results indicate that thermal soaring behaviour increases collision risk with offshore wind farms. Thermal soaring is uncommon relative to the total amount of flight observed, but the propensity for birds to use thermal soaring varies between days, and high peaks in thermal soaring were observed. The correlations between thermal soaring and ΔT and wind components indicate that northerly and north-westerly winds bring in cold air from higher latitudes which increases ΔT and creates opportunities for thermal soaring at sea. This information can be used to predict increased thermal soaring occurrence, which affects collision risk.

Flight altitudes measured in this study agree with previous expectations of gull flight altitude at sea in lesser black-backed gulls (Corman & Garthe 2014, Ross-Smith et al. 2016, Thaxter et al. 2018) and with rates of flight occurring within the RSZ (Ross-Smith et al. 2016). Lesser black-backed gulls using thermal soaring on land at similar latitudes reach much higher altitudes (Sage et al. 2022), which reflects the expected greater strength of thermal uplift on land. Herring gulls have been observed thermal soaring

Table 3. Overview of the logistic regression model parameters for the hourly circling time proportion and hourly circling track proportion measured by GPS and radar, respectively. For each model, estimates and corresponding p-values of model parameters are reported. Models were evaluated with the marginal and conditional R^2_{glmm}

Parameter	Estimate	p	Marginal R^2_{glmm}	Conditional R^2_{glmm}
West radar (n = 2265)				
Intercept	−6.012	<0.001		
Temp. Difference	0.557	<0.001		
			0.207	0.236
Intercept	−5.713	<0.001		
Wind *u*-comp.	0.046	0.022		
Wind *v*-comp.	−0.088	<0.001		
Wind *u*- × *v*-comp.	−0.002	0.746		
			0.038	0.092
West GPS (n = 938)				
Intercept	−4.956	<0.001		
Temp. difference	0.841	<0.001		
			0.483	0.494
Intercept	−4.657	<0.001		
Wind *u*-comp.	0.111	0.004		
Wind *v*-comp.	−0.272	<0.001		
Wind *u*- × *v*-comp.	0.004	0.685		
			0.255	0.275
North radar (n = 866)				
Intercept	−6.625	<0.001		
Temp. difference	0.112	0.127		
			0.006	0.006
Intercept	−6.561	<0.001		
Wind *u*-comp.	0.022	0.310		
Wind *v*-comp.	0.049	0.059		
Wind *u*- × *v*-comp.	−0.011	0.197		
			0.015	0.015
North GPS (n = 586)				
Intercept	−5.438	<0.001		
Temp. Difference	0.819	<0.001		
			0.403	0.403
Intercept	−4.524	<0.001		
Wind *u*-comp.	0.0195	0.581		
Wind *v*-comp.	−0.174	<0.001		
Wind *u*- × *v*-comp.	−0.021	0.054		
			0.170	0.181

over sea from 45 m a.s.l. to altitudes greater than 620 m (Woodcock 1940a, Haney & Lee 1994), and whilst altitudes this high were not observed in our study, they did regularly exceed 100 m and even occasionally 300 m. Considering the lower range of ΔT observed over the North Sea compared to the ΔT range studied by Woodcock (1940a), this is not surprising, as higher ΔT leads to increased uplift (Nourani et al. 2021), and the vertical extent of thermal soaring typically increases with thermal strength and boundary layer depth (Shannon et al. 2002, Shamoun-Baranes et al. 2003).

Studies into the airflow structure within wind farms have shown that the amount of turbulence instigated by wind farms (depending on e.g. wind speed, turbine properties and turbine array layout) can be non-trivial (Stevens & Meneveau 2017), affecting the atmospheric boundary layer and probably thermal uplift. Additionally, soaring birds may adjust their flight behaviour or propensity to use thermals in response to the presence of turbines, as they present obstacles. We found no difference in the probability of thermal soaring within and outside the wind farm in the west, whereas less thermal soaring was detected within the wind farm in the north. However, we note that the mean difference found in the north area was less than 1 bird per square kilometre, and the p-value passes only the most lenient test of significance ($p < 0.05$). Based on these results, it seems that seabirds are not significantly deterred from thermal soaring within wind farms, and we show that thermal uplift within both wind farms was sufficient to soaring flight. Although it is clear that thermal soaring occurs within wind farms, further research is required to uncover the mechanisms and interactions between thermal uplift and thermal soaring within wind farms.

Circling time proportion of lesser black-backed gulls in both study areas and circling track proportion in the radar data of the west area were positively correlated with ΔT and mainly occurred when ΔT was positive. This is consistent with previous findings for gulls at sea (Woodcock 1940a, 1975, Agee & Sheu 1978, Haney & Lee 1994) as well as for migrating raptors and storks observed soaring over sea (Becciu et al. 2020, Nourani et al. 2021). Despite being a temperate sea, positive ΔT conducive to thermal soaring occurred regularly in summer over the southern North Sea, driven by fluctuations in T_a. Most winds (from west, south and east) carry in warm air from the surrounding land masses (Coelingh et al. 1998), but north-westerly winds carry in cold air from higher latitudes, which increases ΔT and creates conditions suitable for thermal soaring. This is confirmed in our results, where thermal soaring probability was highest with northerly and north-westerly winds. The temporal variation of thermal soaring in relation to synoptic conditions demonstrates the important links between synoptic weather patterns and fine-scale flight behaviour. For example, the peaks in thermal soaring activity observed between 20 and 22 July 2020 (Fig. 2) were most likely caused by a cold front passing over the Dutch coast. A trough of low atmospheric pressure followed, bringing in cold air from the north (Section S5 of the Supplement) which decreased T_a and ultimately created favourable conditions for thermal soaring.

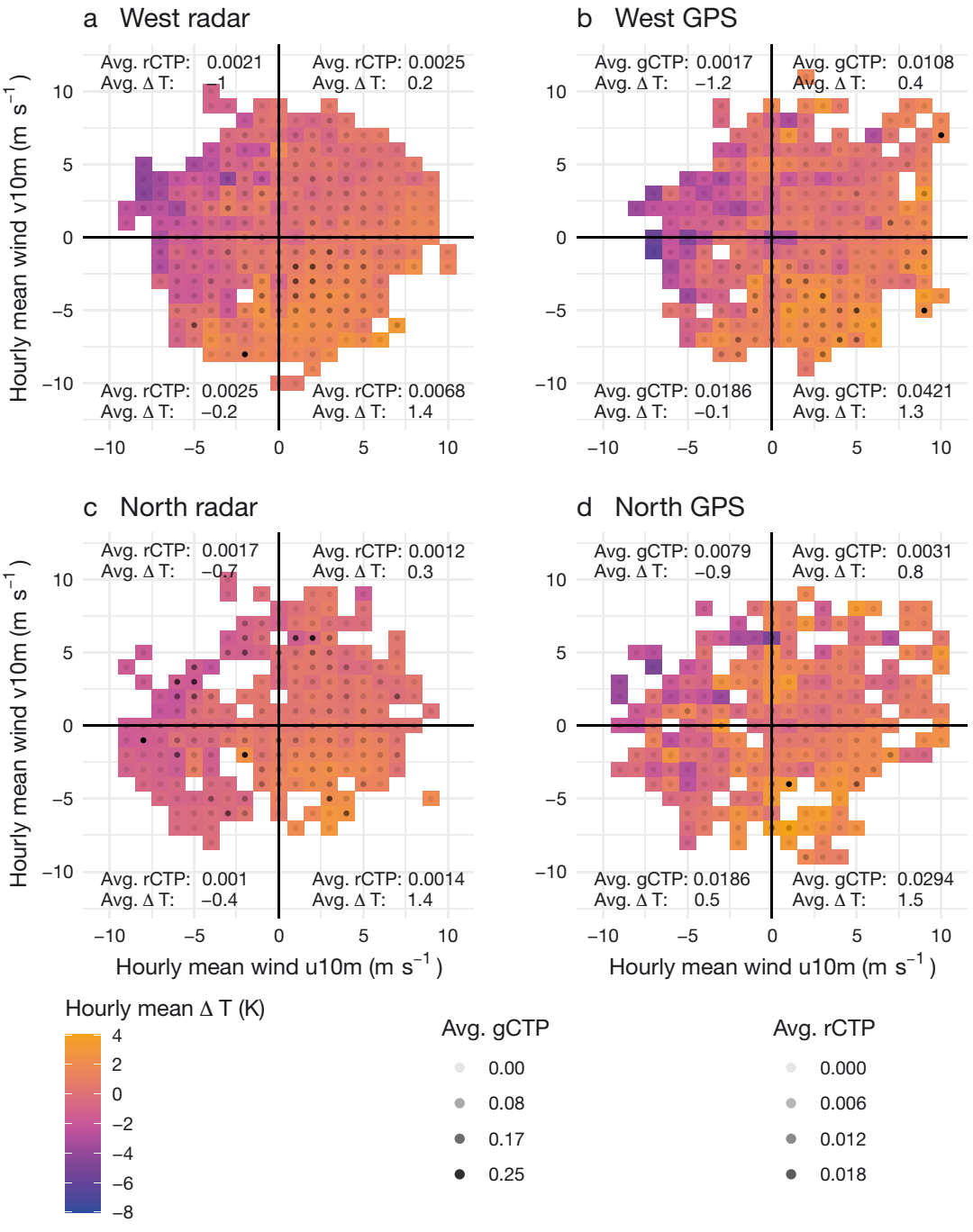

Fig. 6. Average hourly circling track proportion for radar (rCTP) and circling time proportion for GPS (gCTP) binned according to local *u*- and *v*-wind components at 10 m a.s.l. (dots), superimposed on the associated mean ΔT for the same binned wind conditions (coloured tiles). Wind components describe where the winds blow towards, e.g. a positive *u*- and negative *v*-component translates to north-westerly winds. Average circling proportion (Avg. CP) and average temperature difference between sea surface and air at 2 m a.s.l. (Avg. ΔT) per wind quadrant is displayed in the outer corners

Our hypothesis that thermal soaring occurs with positive ΔT was confirmed by the GPS tracking data and the radar data from the west area; however, the north area radar observed very low thermal soaring occurrence, and no significant effect of environmental variables was found. We think limitations of data sampling at the north radar are the main cause for the lack of correlation between ΔT and thermal soaring, rather than a difference in the environmental and behavioural drivers of thermal soaring in the north area.

While the west area radar is situated only 24 km from the mainland, the north area radar is situated 60 km from the nearest land area (Schiermonnikoog). Lesser black-backed gulls rarely travel that far out to sea (Sage 2022), which is also reflected in the low correlation we found between the north GPS and radar data. Additionally, the increased distance from shore means sea state is higher and increased filtering is required to remove clutter from the radar data, which further results in lower track counts. Finally, there are limits to the accuracy of environmental data such as SST which are sensitive to the coupling of the surface and atmosphere (Hristov et al. 2003) and to the influence of land mass in coastal regions (Yao et al. 2021), neither of which is fully accounted for in large reanalysis datasets such as ERA5. Several mismatches where a high circling proportion is measured at relatively low ΔT were observed in the north radar, which is unexpected and could indicate a mismatch between modelled ΔT and local conditions.

As lesser black-backed gulls are the predominant species in both study areas, we attribute most thermal soaring observed by radar to them. Herring gulls are also regularly observed in the west area and are known to use thermal soaring over sea (Woodcock 1940b) and over land (Sage et al. 2022). Other species observed in the study areas, such as great cormorant *Phalocrocorax carbo* (west area) and black-legged kittiwake *Rissa tridactyla* (north area) are not established in the literature to use thermal soaring, although they may have the capacity to do so (Rayner 1988). Discrepancies between circling proportions in GPS and radar on the same day might indicate the presence of other species capable of thermal soaring. Other factors influencing thermal soaring occurrence might be the daily fluctuation in bird abundance at sea (van Erp et al. 2021) and behavioural factors not accounted for in this study. The energy-saving benefits of thermal soaring may be more important for gulls during commuting flight or when searching for aggregations of birds or boats which may signal distant foraging opportunities (Camphuysen 1995), than when foraging on natural prey at the sea surface. Changes in flight motivation may explain why there are many hours with positive ΔT but a low proportion of circling tracks. Future studies of thermal soaring at sea should therefore also seek to incorporate different at-sea behaviours. By integrating knowledge on environmental drivers and intrinsic motivation over multiple seasons, it will become more feasible to predict peaks in thermal soaring and assess the conservation implications, such as the potential influence on collision risk.

Thermal soaring is an important behaviour to study when assessing bird–wind farm interactions. Models of thermal uplift have been used to inform onshore turbine siting decisions on land (Hanssen et al. 2020) and may at some point be appropriate to apply at sea as more knowledge is gathered regarding the spatio-temporal dynamics of thermal soaring offshore. Overall, occurrence of thermal soaring is low relative to total bird flight in our study area in summer. However, we show that specific weather conditions can result in days in which thermal soaring occurrence increases by up to 10 times and flight altitudes increasingly overlap with the RSZ. On 20 July 2020, a peak thermal soaring day, the overall proportion of flight within the RSZ increased to around double the values presented in Table 1 in both north and west areas. Such an increase in flight in the RSZ results in an increased collision risk as estimated by prominent models (Band 2012). The results of this study indicate that peak thermal soaring days can be predicted based on the weather forecast of the region. The increase in thermal soaring proportion and the attributed increase in flight in the RSZ can feed into these models and quantify the increase in collision risk on peak thermal soaring days. Further research should explore the propensity for thermal soaring in a broader range of environments and at different times of the year. Our results indicate thermal soaring at sea occurs rarely, but should environments and periods be identified in which time spent in the RSZ is consistently high as a result of supporting thermal soaring conditions, then marine spatial planning for the region should take this into account.

Combining different information sources to gain a deeper understanding of intricate behavioural patterns and their drivers has been advocated previously (Bauer et al. 2019). There are further strengths of both bio-logging and radar that were not used in this study but could be incorporated into future research. For example, this study only focuses on a 2 mo long summer period, but radar can be used to identify changes in thermal soaring within wind farms throughout the annual cycle, as previous studies have indicated that thermal soaring support can be high in autumn and winter as well (Woodcock 1940a, Haney & Lee 1994). Meanwhile, GPS can be used to examine how individuals incorporate thermal soaring into their daily movement and energy budgets to better understand the ecological impact of thermal soaring. Processing different information sources requires additional expertise and time. Additionally, finding mutual connections by which diverse data sources can be combined (spatially or temporally) is

rarely straightforward. However, by combining the strengths of each measurement technique in a novel approach, we can gain more insight into animal behaviour at a wider spatiotemporal scale, as in this study we gained a better understanding of thermal soaring in remote marine areas and its implication for collision risk than we could have gained through each individual technique.

Acknowledgements. We thank Kees Oosterbeek and the IJmuiden team (Fred Cottaar, Jose Verbeek, Maarten van Kleinwee) for their support on the GPS tagging and tracking measurements at Schiermonnikoog and IJmuiden. We thank PBN and Natuurmonumenten for permission to access the colonies on IJmuiden and Schiermonnikoog, respectively. We thank Rijkswaterstaat (Zee & Delta and Centrale Informatievoorziening) and Gemini wind park for providing the radar data and RobinRadar for providing details on the radar system. The ESAS 5.0 database was queried as a database contributor (K.C.J.C.). Special thanks to Johannes de Groeve, Berend Wijers and Bart Kranstauber for computational help throughout radar data processing. Radar and GPS data analyses were carried out on the Dutch national e-infrastructure with the support of SURF Cooperative. This study is part of the Open Technology Programme, project 'Interactions between birds and offshore wind farms: drivers, consequences and tools for mitigation' (project number 17083), which is financed by the Dutch Research Council (NWO) Domain Applied and Engineering Sciences, in collaboration with public and private partners (Rijkswaterstaat and Gemini wind park).

LITERATURE CITED

Agee EM, Sheu PJ (1978) MCC and gull flight behavior. Boundary-Layer Meteorol 14:247–251

Ainley DG, Porzig E, Zajanc D, Spear LB (2015) Seabird flight behaviour and height in response to altered wind strength and direction. Mar Ornithol 43:25–36

Alerstam T, Rosén M, Bäckman J, Ericson PGP, Hellgren O (2007) Flight speeds among bird species: allometric and phylogenetic effects. PLOS Biol 5:e197

Band B (2012) Using a collision risk model to assess bird collision risks for windfarms. Report for the Crown Estate. British Trust for Ornithology (BTO), Thetford

Bauer S, Shamoun-Baranes J, Nilsson C, Farnsworth A and others (2019) The grand challenges of migration ecology that radar aeroecology can help answer. Ecography 42: 861–875

Becciu P, Rotics S, Horvitz N, Kaatz M and others (2020) Causes and consequences of facultative sea crossing in a soaring migrant. Funct Ecol 34:840–852

Bouten W, Baaij EW, Shamoun-Baranes J, Camphuysen CJ (2013) A flexible GPS tracking system for studying bird behaviour at multiple scales. J Ornithol 154:571–580

Burnham KP, Anderson DR (2002) Model selection and multimodel inference: a practical information-theoretic approach, 2nd edn. Springer-Verlag, New York, NY

Camphuysen CJ (1995) Herring gull *Larus argentatus* and lesser black-backed gull *L. fuscus* feeding at fishing vessels in the breeding season: competitive scavenging versus efficient flying. Ardea 82:365–380

Coelingh JP, van Wijk AJM, Holtslag AM (1998) Analysis of wind speed observations on the North Sea coast. J Wind Eng Ind Aerodyn 73:125–144

Corman AM, Garthe S (2014) What flight heights tell us about foraging and potential conflicts with wind farms: a case study in lesser black-backed gulls (*Larus fuscus*). J Ornithol 155:1037–1043

Croxall JP, Butchart SHM, Lascelles B, Stattersfield AJ, Sullivan B, Symes A, Taylor P (2012) Seabird conservation status, threats and priority actions: a global assessment. Bird Conserv Int 22:1–34

Esteban M, Leary D (2012) Current developments and future prospects of offshore wind and ocean energy. Appl Energy 90:128–136

European Commission (2020) Offshore renewable energy for a climate-neutral Europe. https://eur-lex.europa.eu/legal-content/EN/TXT/?uri=COM%3A2020%3A741%3AFIN. https://eur-lex.europa.eu/legal-content/EN/TXT/?uri=COM%3A2020%3A741%3AFIN

Haney JC, Lee DS (1994) Air-sea heat flux, ocean wind fields, and the offshore dispersal of gulls. Auk 111:427–440

Hanssen F, May R, Nygård T (2020) High-resolution modeling of uplift landscapes can inform micrositing of wind turbines for soaring raptors. Environ Manag 66: 319–332

Hersbach H, Bell B, Berrisford P, Hirahara S and others (2020) The ERA5 global reanalysis. Q J R Meteorol Soc 146:1999–2049

Hersbach H, Bell B, Berrisford P, Horányi A and others (2022) ERA5 hourly data on single levels from 1940 to present. Copernicus Climate Change Service (C3S) Climate Data Store (CDS), doi:10.24381/cds.adbb2d47 (accessed 10 February 2022)

Hristov TS, Miller SD, Friehe CA (2003) Dynamical coupling of wind and ocean waves through wave-induced air flow. Nature 422:55–58

Johnston A, Cook ASCP, Wright LJ, Humphreys EM, Burton NHK (2014) Modelling flight heights of marine birds to more accurately assess collision risk with offshore wind turbines. J Appl Ecol 51:31–41

Kleyheeg-Hartman JC, Krijgsveld KL, Collier MP, Poot MJM, Boon AR, Troost TA, Dirksen S (2018) Predicting bird collisions with wind turbines: comparison of the new empirical Flux Collision Model with the SOSS Band model. Ecol Model 387:144–153

Krijgsveld KL, Fijn RC, Heunks C, van Horssen PW and others (2011) Effect studies offshore wind farm Egmond aan Zee. Progress report on fluxes and behaviour of flying birds. Rep No. 08-028. Bureau Waardenburg, Culemborg

Lindhe Norberg UM (2002) Structure, form, and function of flight in engineering and the living world. J Morphol 252:52–81

Marques AT, Batalha H, Rodrigues S, Costa H and others (2014) Understanding bird collisions at wind farms: an updated review on the causes and possible mitigation strategies. Biol Conserv 179:40–52

Nakagawa S, Johnson PCD, Schielzeth H (2017) The coefficient of determination R^2 and intra-class correlation coefficient from generalized linear mixed-effects models revisited and expanded. J R Soc Interface 14:20170213

NOAH (2022) North Sea observation and assessment of habitats. https://www.noah-project.de/habitatatlas/index.php.en (accessed 1 February 2022)

Nourani E, Yamaguchi NM (2017) The effects of atmos-

pheric currents on the migratory behavior of soaring birds: a review. Ornitholog Sci 16:5–15
Nourani E, Vansteelant WMG, Byholm P, Safi K (2020) Dynamics of the energy seascape can explain intra-specific variations in sea-crossing behaviour of soaring birds. Biol Lett 16:20190797
Nourani E, Bohrer G, Becciu P, Bierregaard RO and others (2021) The interplay of wind and uplift facilitates over-water flight in facultative soaring birds. Proc R Soc B 288: 20211603
Pennycuick BYCJ (1983) Thermal soaring compared in three dissimilar tropical bird species, *Fregata magnificens*, *Pelecanus occidentalis* and *Coragyps atratus*. J Exp Biol 102:307–326
Pennycuick CJ (2008) Modelling the flying bird. Academic Press, London
Péron G, Fleming CH, Duriez O, Fluhr J and others (2017) The energy landscape predicts flight height and wind turbine collision hazard in three species of large soaring raptor. J Appl Ecol 54:1895–1906
Perrow MR (2019) Wildlife and wind farms — conflicts and solutions, Vol 3. Pelagic Publishing, Exeter
R Core Team (2022) R: a language and environment for statistical computing. R Foundation for Statistical Computing, Vienna
Rayner JMV (1988) Form and function in avian flight. Curr Ornithol 5:1–66
Reid J, Camphuysen CJ (1998) The European Seabirds at Sea database. In: Spina S, Grattarola A (eds) Proc 1st Meet European Ornithologists' Union. Biol Cons Fauna 102:291
Rijksoverheid (2019) Klimaatakkoord. https://www.rijksoverheid.nl/onderwerpen/klimaatverandering/documenten/rapporten/2019/06/28/klimaatakkoord (accessed 3 February 2022)
Ross-Smith VH, Thaxter CB, Masden EA, Shamoun-Baranes J and others (2016) Modelling flight heights of lesser black-backed gulls and great skuas from GPS: a Bayesian approach. J Appl Ecol 53:1676–1685
Sage E (2022) Wind energy for all! The dynamic flight of gulls in human-engineered landscapes. PhD thesis, University of Amsterdam
Sage E, Bouten W, Hoekstra B, Camphuysen KCJ, Shamoun-Baranes J (2019) Orographic lift shapes flight routes of gulls in virtually flat landscapes. Sci Rep 9:9659
Sage E, Bouten W, van Dijk W, Camphuysen KCJ, Shamoun-Baranes J (2022) Built up areas in a wet landscape are stepping stones for soaring flight in a seabird. Sci Total Environ 852:157879
Shamoun-Baranes J, Leshem Y, Yom-Tov Y, Liechti O (2003) Differential use of thermal convection by soaring birds over central Israel. Condor 105:208–218
Shamoun-Baranes J, van Loon E, Liechti F, Bouten W (2007) Analyzing the effect of wind on flight: pitfalls and solutions. J Exp Biol 210:82–90
Shamoun-Baranes J, Bouten W, van Loon EE, Meijer C, Camphuysen CJ (2016) Flap or soar? How a flight generalist responds to its aerial environment. Philos Trans R Soc B 371:20150395
Shannon HD, Young GS, Yates MA, Fuller MR, Seegar WS (2002) American white pelican soaring flight times and altitudes relative to changes in thermal depth and intensity. Condor 104:679–683
Spear LB, Ainley DG (1997a) Flight speed of seabirds in relation to wind speed and direction. Ibis 139:234–251
Spear LB, Ainley DG (1997b) Flight behaviour of seabirds in relation to wind direction and wing morphology. Ibis 139: 221–233
Stevens RJAM, Meneveau C (2017) Flow structure and turbulence in wind farms. Annu Rev Fluid Mech 49:311–339
Thaxter CB, Ross-Smith VH, Bouten W, Masden EA and others (2018) Dodging the blades: new insights into three-dimensional area use of offshore wind farms by lesser black-backed gulls *Larus fuscus*. Mar Ecol Prog Ser 587: 247–253
Thaxter CB, Ross-Smith VH, Bouten W, Clark NA and others (2019) Avian vulnerability to wind farm collision through the year: insights from lesser black-backed gulls (*Larus fuscus*) tracked from multiple breeding colonies. J Appl Ecol 56:2410–2422
Treep J, Bohrer G, Shamoun-Baranes J, Duriez O, Prata de Moraes Frasson R, Bouten W (2016) Using high resolution GPS tracking data of bird flight for meteorological observations. Bull Am Meteorol Soc 97:951–961
van Erp JA, van Loon EE, Camphuysen CJC, Shamoun-Baranes J (2021) Temporal patterns in offshore bird abundance during the breeding season at the Dutch North Sea coast. Mar Biol 168:150
Venables WN, Ripley BD (2002) Modern applied statistics with S, 4th edn. Springer, New York, NY
Weimerskirch H, Chastel O, Barbraud C, Tostain O (2003) Flight performance: Frigatebirds ride high on thermals. Nature 421:333–334
Weimerskirch H, Bishop C, Jeanniard-du-Dot T, Prudor A, Sachs G (2016) Frigate birds track atmospheric conditions over months-long transoceanic flights. Science 353: 74–78
Weinzierl R, Bohrer G, Kranstauber B, Fielder W, Wikelski M, Flack A (2016) Wind estimation based on thermal soaring of birds. Ecol Evol 6:8706–8718
Woodcock AH (1940a) Convection and soaring over the open sea. J Mar Res 3:248–253
Woodcock AH (1940b) Observations on herring gull soaring. Auk 57:219–224
Woodcock AH (1975) Thermals over the sea and gull flight behavior. Boundary-Layer Meteorol 9:63–68
Yamaguchi NM, Arisawa Y, Shimada Y, Higuchi H (2012) Real-time weather analysis reveals the adaptability of direct sea-crossing by raptors. J Ethol 30:1–10
Yao L, Lu J, Xia X, Jing W, Liu Y (2021) Evaluation of the ERA5 sea surface temperature around the Pacific and the Atlantic. IEEE Access 9:12067–12073

Editorial responsibility: Thomas A. Clay (Guest Editor), Santa Cruz, California, USA
Reviewed by: E. Lempidakis, F. Liechti and 1 anonymous referee

Submitted: July 7, 2022
Accepted: April 19, 2023
Proofs received from author(s): June 12, 2023